Interaction of Strong Single-Cycle Terahertz Pulses with Semiconductor Quantum Wells

J. R. Danielson,[1] Yun-Shik Lee,[1,*] J. P. Prineas,[2] J. T. Steiner,[3] M. Kira,[3] and S. W. Koch[3]

[1]*Department of Physics, Oregon State University, Corvallis, Oregon 97331, USA*
[2]*Department of Physics and Astronomy, University of Iowa, Iowa City, Iowa 52242, USA*
[3]*Department of Physics and Material Sciences Center, Philipps-University, 35032 Marburg, Germany*

(Received 12 June 2007; published 3 December 2007)

An experiment-theory comparison is presented to demonstrate terahertz-induced extreme-nonlinear transients in a GaAs/AlGaAs quantum-well system. The terahertz-pump and optical-probe experiments show pronounced spectral modulations of the light- and heavy-hole excitonic resonances. Excellent agreement with the results of microscopic many-body calculations is obtained, identifying clear ponderomotive contributions and the generation of terahertz harmonics.

DOI: 10.1103/PhysRevLett.99.237401 PACS numbers: 78.67.De, 42.50.Hz, 42.65.Ky, 71.35.−y

In recent years, the development of coherent terahertz (THz) sources has established a new regime of semiconductor optics where internal transitions between quasiparticle states can be probed directly. Investigations have employed time-resolved spectroscopy with weak THz pulses to detect and monitor conductivity [1], the buildup of plasma screening [2], and bound exciton formation [3–7]. In parallel, it has been shown that the application of intense THz fields to semiconductors strongly modifies and controls the optical properties [8–21].

In this context, it is interesting to study excitation of a semiconductor quantum well (QW) with an intense single-cycle THz pulse whose Rabi energy approaches the energy of the excitonic $1s$-to-$2p$ transition. Such investigations enter the regime of extreme-nonlinear optics [13,22] where the rotating-wave approximation (RWA) breaks down. Instead, the light-induced transitions depend on both the envelope of the THz pulse and its carrier-envelope offset phase [23]. Furthermore, the contributions beyond the RWA lead to high harmonics in the spectrum. The extreme-nonlinear dynamics induced by THz excitation of a QW is particularly interesting since, in contrast to optical excitation in this regime [24], Coulomb effects remain important. Thus, new insights into the internal dynamics of excitonic QW polarization can be obtained.

In this Letter, we present an experiment-theory investigation of a pump-probe measurement with a strong single-cycle THz pulse and a weak optical probe to study time-resolved nonlinear effects in the optical spectrum in multiple GaAs/AlGaAs QWs. The schematic experimental setup is shown in Fig. 1(a). The measurements were performed using 805-nm, 100-fs pulses from a 1-kHz Ti:sapphire regenerative amplifier (Coherent Inc., Legend). The optical beam was split into two components: the major portion for THz generation and the minor portion for the optical probe. Single-cycle THz pulses were generated by optical rectification in a 1-mm ZnTe crystal. The incident optical pulse energy was 0.8 mJ, irradiated on a roughly 3-mm spot in the ZnTe crystal. The THz pulses were collimated with an off-axis parabolic mirror and the THz beam diameter was 1.5 mm at the focus. The THz pulse shape was measured using electro-optic sampling in a 1-mm ZnTe crystal. We also determined the absolute THz power using a Si bolometer at liquid He temperature. The THz electric-field amplitude at the peak is estimated as 10 kV/cm when the optical pump-pulse energy is 0.8 mJ.

We put a GaAs QW sample at the focus of the THz pulses and measured optical transmission spectra. The sample studied has ten high-quality, undoped 12-nm-wide GaAs QWs separated by 16-nm-wide $Al_{0.3}Ga_{0.7}As$ barriers. The measured $1 - T(\omega)$ spectrum of the sample, where $T(\omega)$ is the spectrally resolved linear transmission probability of the optical field, is shown as a shaded area in Fig. 1(b). This spectrum is analyzed combining our standard microscopic theory [25] with a $\mathbf{k} \cdot \mathbf{p}$-band-structure calculation including the HH and LH valence bands as well as the strain inside the sample. The results are shown as a solid line in Fig. 1(b).

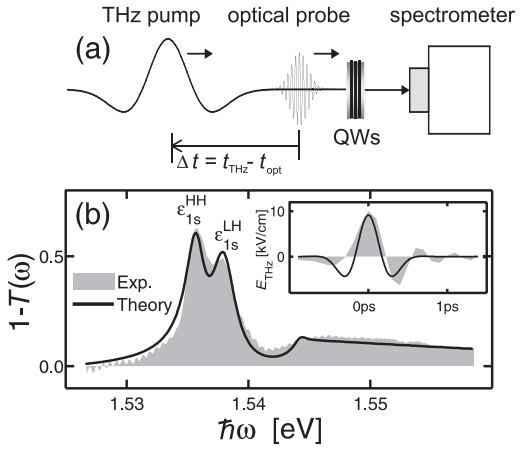

FIG. 1. (a) Experimental setup. (b) Experimental (shaded area) and theoretical (solid line) $1 - T(\omega)$. The $1s$-HH (heavy-hole) and LH (light-hole) resonances are at $\varepsilon_{1s}^{HH} = 1.536$ eV and $\varepsilon_{1s}^{LH} = 1.538$ eV, respectively. The inset shows the electric field of the experimental (shaded area) and theoretical (solid line) THz pulse.

 © 2007 The American Physical Society

The sample is excited by strong THz pulses [Fig. 1(b) inset] and probed by weak optical pulses having central times t_{THz} and t_{opt}, respectively. We measure the spectrally resolved intensity of the optical pulse as function of the delay $\Delta t = t_{\mathrm{THz}} - t_{\mathrm{opt}}$ yielding the normalized transmission probability $T(\omega, \Delta t)$. The THz-induced changes are obtained as the differential spectrum $\Delta T \equiv T(\omega) - T(\omega, \Delta t)$.

The description of the nonlinear experiment follows from the standard many-body Hamiltonian [25] for the Coulomb-interacting carriers that are coupled to light via the minimal-substitution Hamiltonian [26–29]. To obtain the optical response under the influence of an intense THz excitation, we solve the generalized multiband semiconductor-Bloch equations for the microscopic polarization $P_{\mathbf{k}}^{\alpha}$ with carrier momentum $\mathbf{k}$ between conduction band and valence band α:

$$i\hbar \frac{\partial}{\partial t} P_{\mathbf{k}}^{\alpha} = \left(\varepsilon_{\mathbf{k}}^{\alpha} - j_{\mathbf{k}}^{\alpha} A_{\mathrm{THz}} + \frac{e^2}{2\mu^{\alpha}} A_{\mathrm{THz}}^2 \right) P_{\mathbf{k}}^{\alpha} - (1 - f_{\mathbf{k}}^{e} - f_{\mathbf{k}}^{h,\alpha}) \left[d_{\mathbf{k}}^{\alpha} E_{\mathrm{opt}} + \sum_{\mathbf{k}'} V_{\mathbf{k}-\mathbf{k}'}^{\alpha} P_{\mathbf{k}'}^{\alpha} \right] + \text{scattering}. \quad (1)$$

Here, $\varepsilon_{\mathbf{k}}^{\alpha}$ contains the kinetic energy of the single conduction- and multiple valence-band carriers having occupations $f_{\mathbf{k}}^{e}$ and $f_{\mathbf{k}}^{h,\alpha}$, respectively. Furthermore, $d_{\mathbf{k}}^{\alpha}$ is the interband dipole-matrix element, $j_{\mathbf{k}}^{\alpha} \equiv -|e|/\hbar \partial \epsilon_{\mathbf{k}}^{\alpha} / \partial |\mathbf{k}| \cos\phi_{\mathbf{k}}$ is the current-matrix element with the angle $\phi_{\mathbf{k}}$ between $\mathbf{k}$ and the polarization direction of the THz field, and μ^{α} is the effective reduced mass [29,30]. We evaluate $\varepsilon_{\mathbf{k}}^{\alpha}$, $d_{\mathbf{k}}^{\alpha}$, $j_{\mathbf{k}}^{\alpha}$, μ^{α}, and the Coulomb-matrix element $V_{\mathbf{k}}^{\alpha}$ using the wave functions from our $\mathbf{k} \cdot \mathbf{p}$-band-structure calculation. The presence of carriers and the coupling to phonons and disorder lead to scattering of the polarization. Since excitation-induced dephasing [28,31] is not appreciable for the weak optical excitation used, we implement scattering via a constant dephasing.

The polarization couples to both the optical electric field E_{opt} and the THz vector potential A_{THz} at the QW position. The term proportional to dE_{opt} describes the optical generation of polarization whereas the two terms containing A_{THz} describe intraband processes. The A^2-dependent renormalization of the kinetic energies is always positive, and it can be directly related to the so-called ponderomotive energy [8] which is the average kinetic energy of a charged classical particle in a harmonic electromagnetic field.

The strong THz pulse couples to the optical polarization via the $j^{\alpha} A_{\mathrm{THz}}$ term that has a different parity than the purely optically generated polarization since $j_{-\mathbf{k}} = -j_{\mathbf{k}}$. Thus, the experimental single-cycle THz pulse converts the initially s-like polarization into p-, d-, ... like contributions via linear and nonlinear transitions. The transition frequencies between the different excitonic states fall into the region of a few THz, e.g., $\nu_{2p}^{\mathrm{HH}} - \nu_{1s}^{\mathrm{HH}} = 1.96$ THz and $\nu_{2p}^{\mathrm{LH}} - \nu_{1s}^{\mathrm{LH}} = 1.65$ THz, where $\varepsilon_{\lambda} = h\nu_{\lambda}$ is the energy of state λ. These THz-induced transitions can be observed as large changes in the differential spectrum $\Delta T(\omega, \Delta t)$.

We treat the light propagation through the experimental multi-QW structure by solving Maxwell's wave equation via a transfer-matrix technique [32]. The theoretical $A_{\mathrm{THz}}(t) = A_0 \exp[-(t/\tau)^2] \cos(2\pi\nu_{\mathrm{THz}} t + \phi)$ is matched to the experimental single-cycle THz pulse choosing the central frequency $\nu_{\mathrm{THz}} = 0.9$ THz, carrier-envelope offset phase $\phi = \pi/2$, duration $\tau = 300$ fs, and A_0 such that the peak strength of the electric field is 9.2 kV/cm.

At the pulse peak we realize the ratios $\nu_R^{\mathrm{HH}}/\nu_{2p1s}^{\mathrm{HH}} = 0.63$ and $\nu_R^{\mathrm{LH}}/\nu_{2p1s}^{\mathrm{LH}} = 0.79$ between the Rabi energy $h\nu_R$ and the $1s$-$2p$ transition energy. These values are clearly in the regime of extreme-nonlinear optics where one expects ultrafast nonlinearities.

Figures 2(a) and 3(a) present the experimental and theoretical ΔT as a function of optical energy $\hbar\omega$ and time delay Δt. The horizontal lines indicate energy cross sections, and the vertical lines represent time slices for fixed energies. A comparison of Figs. 2 and 3 shows that the theory excellently reproduces not only the magnitude of the essential features in ΔT, but also their spectral and temporal shapes.

We note that the THz-induced features are strong—changes are almost 50% of the linear T in Fig. 1(b)—and several transient ΔT signatures appear on an ultrafast subpicosecond time scale. As we discuss in the following paragraphs, the experimental signal contains well-defined characteristics of (i) ponderomotive contributions, (ii) signatures of the excitonic dynamical Franz-Keldysh effect [9], as well as (iii) large deviations from the RWA including THz harmonic generation. Performing a detailed switch-off analysis, the theory clearly identifies the physical origin of the different ΔT contributions.

In both Figs. 2(a) and 3(a), we observe for small time delays $\Delta t_b = 0.22$ ps, energetically slightly above the $1s$-LH resonance at $\hbar\omega_e = 1.540$ eV, a positive ΔT (white region with arrow) that exists transiently for about 500 fs—shorter than the other transients around the $1s$ resonances. In cross sections (b) and (e) in Figs. 2 and 3 this feature is indicated by an arrow. To reveal its origin, Figs. 3(b) and 3(e) compare the full computation (shaded area) with calculations where either the A^2 term in Eq. (1) is switched off (dashed line) or the RWA is applied (solid line). We see that without the A^2 term the positive ultrafast ΔT feature is nearly washed out and the overall shape of the experimental ΔT is not reproduced at all. Thus, we can directly link this ultrafast transient to the presence of the ponderomotive A^2 contribution of the single-cycle THz pulse. As we discussed after Eq. (1), the A^2 term can be interpreted classically as the kinetic-energy change of the electron in a strong electromagnetic field. Thus, the distinct feature can be understood intuitively as evidence of the

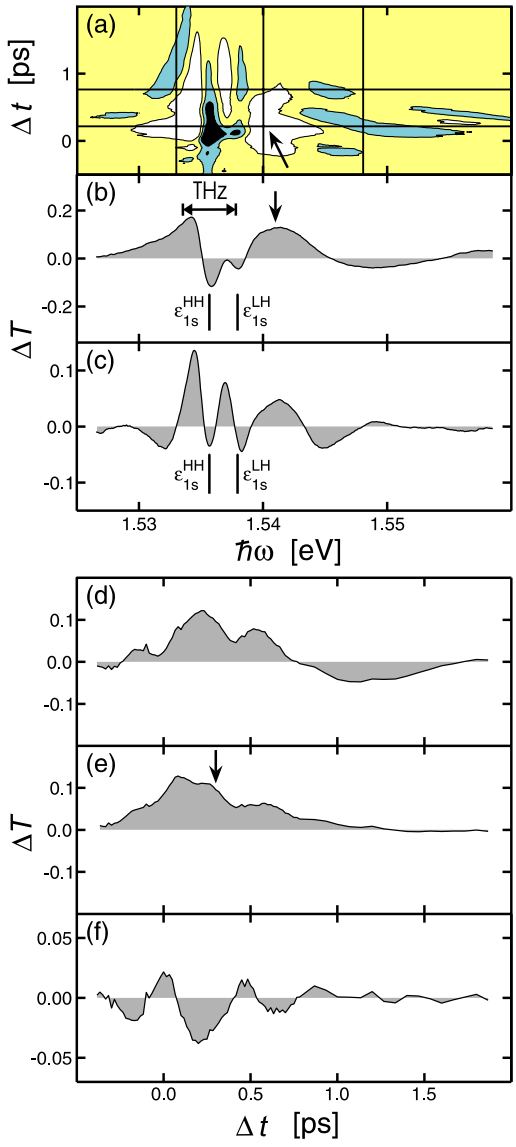

FIG. 2 (color online). Experimental differential spectrum. (a) Contour plot of $\Delta T(\omega, \Delta t)$. Contour lines are depicted for the values -0.07, -0.02, and $+0.04$; the color becomes lighter for larger values. The horizontal black lines correspond to cross sections at $\Delta t_b = 0.22$ ps and $\Delta t_c = 0.78$ ps shown as a shaded area in (b) and (c), respectively. The black vertical lines correspond to cross sections for $\hbar\omega_d = 1.533$ eV, $\hbar\omega_e = 1.540$ eV, and $\hbar\omega_f = 1.548$ eV which are shown as a shaded area in (d), (e) and (f), respectively. The horizontal bar in (b) denotes the full width at half maximum of the THz spectrum.

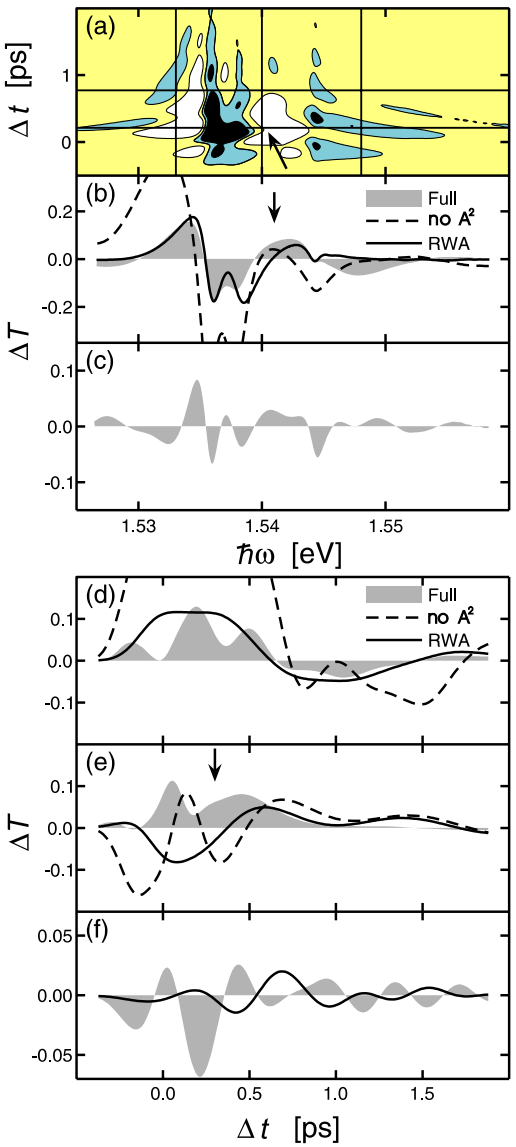

FIG. 3 (color online). Theoretical differential spectrum. The contour lines and the position of the cross sections are the same as in Fig. 2. In addition to the results of the full computation (shaded area), (b), (d,) and (e) show the results with the A^2 term switched off (dashed line) and (b), (d), (e), and (f) show the results when the RWA is applied (solid line).

electron's ''wiggle'' energy due to the strong THz field. As this energy is quadratic in A_{THz}, it is clear that this feature is shorter-lived than the other transients. Besides this, we find that the non-RWA contributions are needed to obtain the correct oscillatory shape of ΔT around the ponderomotive ΔT transient. Thus, the extreme nonlinearity of the induced ΔT feature is clearly demonstrated.

In both experiment and theory, the shape of ΔT suggests that the excitonic $1s$-HH resonance in T is redshifted, whereas the $1s$-LH resonance in T is blueshifted for early and redshifted for later delay times due to the THz pulse. Comparing in Fig. 3(b) calculations with (shaded area) and without (dashed line) the A^2 term shows that the ponderomotive term contributes as a compensating blueshift. In particular, the blueshift of the excitonic $1s$-LH resonance in T for early delay times can be explained only when the A^2 term is included. These observations are in agreement with earlier investigations [8–10] of the excitonic dynamical Franz-Keldysh effect for continuous-wave THz excitations. For small delay times, the THz interaction with the optical polarization is strongest and the ponderomotive A^2

dominates causing an overall blueshift for the $1s$-LH resonance. At later delay times, the ac-Stark shift dominates yielding an overall redshift for both resonances.

Figure 3(d) displays the temporal evolution of ΔT at the energy $\hbar\omega_d = 1.533$ eV that is below the $1s$-HH resonance. Again, the full computation (shaded area) reproduces the experimentally measured [Fig. 2(d)] features. When we switch off either the A^2 contribution (dashed line) or apply the RWA (solid line), the result no longer agrees with the experiment. We observe again that the A^2 and the jA contributions compensate each other. In addition, the fast oscillations in ΔT induced by non-RWA parts clearly indicate that the experiment is in the regime of extreme-nonlinear excitations as the dynamics is determined by the full oscillations of the THz pulse and not only by its envelope. The theoretical analysis confirms that the actual positions of the oscillations in ΔT can be controlled by the carrier-envelope offset phase.

As a last feature, we investigate ΔT at $\hbar\omega_f = 1.548$ eV, where shallow resonance features are centered at the energy matching $\varepsilon_{1s} + \Delta/2 + 2h\nu_{\mathrm{THz}}$, where Δ is the detuning of the THz pulse with respect to the $1s$-$2p$ transition. Since the THz spectrum—the bar in Fig. 2(b) indicates the full width at half maximum—is much narrower than the extension of the high energy features, we can rule out the explanation that they arise due to absorption of a single THz photon. Thus, these features clearly result from THz third harmonic generation since one needs the absorption of two additional THz photons, a contribution which is neglected in the RWA. Figure 3(f) presents $\Delta T(\omega_f, \Delta t)$ for the full computation (shaded area) and with the RWA (solid line). Only residual oscillations are observed with the RWA; for slightly longer THz pulses these residual oscillations vanish altogether. Since the oscillatory features are at the correct energetic position and require non-RWA contributions, also these experimental features can be connected to extreme nonlinearities. Our theoretical analysis shows that the positions of the Δt-dependent oscillations of ΔT depend on the carrier-envelope offset phase ϕ and that the spectral position depends on the central frequency of the THz pulse [14].

In conclusion, we performed experimental and theoretical investigations of the interaction of strong single-cycle THz pulses with semiconductor QWs. The measured spectra are excellently reproduced by the results of our microscopic calculations. A detailed switch-off analysis clearly identifies extreme-nonlinear effects including ponderomotive contributions and THz harmonics.

The Marburg work is supported by the Quantum Optics in Semiconductors DFG Research Group. The OSU group is supported by NSF CAREER Grant No. 0449426.

*leeys@physics.oregonstate.edu

[1] R. H. M. Groeneveld and D. Grischkowsky, J. Opt. Soc. Am. B **11**, 2502 (1994).
[2] R. Huber *et al.*, Nature (London) **414**, 286 (2001).
[3] R. A. Kaindl *et al.*, Nature (London) **423**, 734 (2003).
[4] I. Galbraith *et al.*, Phys. Rev. B **71**, 073302 (2005).
[5] M. Kira *et al.*, Phys. Rev. Lett. **87**, 176401 (2001).
[6] M. Kira, W. Hoyer, and S. W. Koch, Solid State Commun. **129**, 733 (2004).
[7] S. W. Koch *et al.*, Nature Mater. **5**, 523 (2006).
[8] A. P. Jauho and K. Johnsen, Phys. Rev. Lett. **76**, 4576 (1996).
[9] K. B. Nordstrom *et al.*, Phys. Rev. Lett. **81**, 457 (1998).
[10] S. Hughes and D. S. Citrin, Phys. Rev. B **59**, R5288 (1999).
[11] A. H. Chin, J. M. Bakker, and J. Kono, Phys. Rev. Lett. **85**, 3293 (2000).
[12] B. Cole *et al.*, Nature (London) **410**, 60 (2001).
[13] A. H. Chin, O. G. Calderón, and J. Kono, Phys. Rev. Lett. **86**, 3292 (2001).
[14] C. J. Dent, B. N. Murdin, and I. Galbraith, Phys. Rev. B **67**, 165312 (2003).
[15] A. Srivastava *et al.*, Phys. Rev. Lett. **93**, 157401 (2004).
[16] A. V. Maslov and D. S. Citrin, Phys. Rev. B **62**, 16 686 (2000).
[17] T. Müller *et al.*, Appl. Phys. Lett. **84**, 64 (2004).
[18] C. W. Luo *et al.*, Phys. Rev. Lett. **92**, 047402 (2004).
[19] S. G. Carter *et al.*, Science **310**, 651 (2005).
[20] J. F. Dynes *et al.*, Phys. Rev. Lett. **94**, 157403 (2005).
[21] D. Stehr *et al.*, Appl. Phys. Lett. **88**, 151108 (2006).
[22] O. D. Mücke *et al.*, Phys. Rev. Lett. **89**, 127401 (2002).
[23] M. Wegener, *Extreme Nonlinear Optics* (Springer, New York, 2006).
[24] D. Golde, T. Meier, and S. W. Koch, J. Opt. Soc. Am. B **23**, 2559 (2006).
[25] H. Haug and S. W. Koch, *Quantum Theory of the Optical and Electronic Properties of Semiconductors* (World Scientific, Singapore, 2004), 4th ed.
[26] C. Cohen-Tannoudji, J. Dupont-Roc, and G. Grynberg, *Photons and Atoms—Introduction to Quantum Electrodynamics* (Wiley, New York, 1989), 3rd ed.
[27] M. Kira *et al.*, Prog. Quantum Electron. **23**, 189 (1999).
[28] M. Kira and S. W. Koch, Prog. Quantum Electron. **30**, 155 (2006).
[29] M. Kira, W. Hoyer, and S. W. Koch, Phys. Status Solidi (b) **238**, 443 (2003).
[30] J. M. Luttinger and W. Kohn, Phys. Rev. **97**, 869 (1955).
[31] F. Jahnke *et al.*, Phys. Rev. Lett. **77**, 5257 (1996).
[32] F. Jahnke *et al.*, in *Advances in Solid State Physics*, edited by R. Helbig (Vieweg, Braunschweig/Wiesbaden, 1998), Vol. 37, p. 191.